Thermodynamical stability of carbon-based defects in α boron from first principles

Yeonsoo Cho, Jelena Sjakste, Olivier Hardouin Duparc, Nathalie Vast

Highlights

Thermodynamical stability of carbon-based defects in α boron from first principles

Yeonsoo Cho, Jelena Sjakste, Olivier Hardouin Duparc, Nathalie Vast

- May 24, 2024
- Exhaustive study of the formation enthalpy and charge states of carbon-based defects in rhombohedral α boron.
- In the basal plane, two interstitial carbon atoms tend to form a puckered B_4C_2 hexagon with boron atoms of surrounding icosahedra.
- The defect stability of two interstitial carbon atoms along the rhombohedral axis is shown to be controlled by the distance between the carbon atoms. Additional negative charges stabilize the carbon–carbon diatomic chain.

Thermodynamical stability of carbon-based defects in α boron from first principles

Yeonsoo Cho[a], Jelena Sjakste[a], Olivier Hardouin Duparc[a], Nathalie Vast[a]

[a]*Laboratoire des Solides Irradiés, École Polytechnique, CEA/DRF/IRAMIS, CNRS UMR 7642, Institut Polytechnique de Paris, 28 Route de Saclay, F-91128, Palaiseau Cedex, France*

Abstract

We report an exhaustive study of the formation enthalpy and charge states of carbon-based defects in rhombohedral α boron within the density functional theory (DFT) that enables us to derive rules about the formation of complex carbon defects. We have accounted for one and two interstitial carbon atoms, eventually combined with one substitutional carbon atom and/or one interstitial boron atom and varied several geometric parameters. We find that when positioned in the plane perpendicular to the [111] rhombohedral axis, two carbon atoms turn out to preferentially form a graphite-like hexagon with four boron atoms. When positioned instead along the [111] axis, the distance between them strongly affects the defect thermodynamic stability, and we find in particular that additional negative charges strongly stabilize the diatomic carbon–carbon chains.

1. Introduction

The main incentive to study carbon-based point defects in α boron that have low formation enthalpy is the expectation to better understand the stability of the various polymorphs of elemental boron, since the thermodynamically stable phase, β boron, is thought to be stabilized by intrinsic point defects [1]. Indeed, the recent study of point defects in boron rich phases with a similar crystal structure, boron carbide, has led to important conclusions on phase stability [2, 3, 4].

On the practical side, the main obstacle for such studies - the absence of a viable route for mass production of α boron - has recently been lifted by the discovery that the presence of carbon atoms triggers the formation of α boron in high pressure and high temperature syntheses, with potential

Email addresses: yeonsoo.cho@polytechnique.edu (Yeonsoo Cho), jelena.sjakste@polytechnique.edu (Jelena Sjakste), olivier.hardouinduparc@polytechnique.edu (Olivier Hardouin Duparc), nathalie.vast@polytechnique.edu (Nathalie Vast)

presence of carbon impurities in α boron [5]. This has clearly been shown by comparing three samples: one that solely contained crystalline β boron; another one that contained crystalline β boron and amorphous carbon; and the last one that contained amorphous boron and amorphous carbon. Only in the latter two samples had α boron formed, at pressure (P) and temperature (T) values studied in Ref. [5]. Computations of the equilibrium volume of carbon impurities in α boron have been compared to experiments that have led to the conclusion that some carbon impurities exist in the α boron formed in the above-mentioned conditions. The main scope of the present work is thus to find a method to classify carbon- and boron-based defects in α boron and derive general rules regarding the effect of defect geometry on their thermodynamic stability. We rely on calculations performed within the density functional theory (DFT) to compute the formation enthalpy, varying the number of interstitial and substitutional carbon and boron atoms, and their geometry.

We aim at deepening the fundamental knowledge about point defects in α boron. The latter is known to be semiconducting, to show up as a red crystal [6, 7, 8, 9] and to have a band gap of 2 eV [10]. We note, however, that experimentally prepared crystals of α boron, depending on the synthesis conditions, have shown colors other than red, such as black [6, 7], orange or light yellow [11]. This may tentatively be attributed to the presence of point defects - impurities - in the crystalline structure, although a deep and general understanding is still missing. Present state of the art about point defects in α boron consists mainly in theoretical studies of the atomic structure doped with lithium (Li) atoms [12, 13, 14, 15, 16, 17], hydrogen (H) atoms [18], or magnesium (Mg) atoms [14], and has mostly targeted potential superconductivity properties of doped α boron. Defects containing one carbon atom have been studied with *ab initio* calculations, with the purpose to explain the experimental data of Ref. [5]. Yet, a general framework for the classification of point defects in α boron is still missing, in wide contrast to the β boron allotrope [19, 20, 1] and icosahedral boron carbide [21, 22, 23, 24, 2, 3, 4].

In Section 2, we describe the computational method for the modeling of defects. In Sections 3 and 4, we show results on the stability of neutral and charged defects, respectively. Conclusions about rules of formation of complex carbon-defects in the atomic structure of α boron are drawn in Section 5.

2. Methods

2.1. Design of defect models and definition of the atomic geometry

Guided by the fact that α boron turns out to be an intermediate phase occurring before the formation of B_4C [25], we have repeated the pristine rhombohedral unit cell, which contains twelve B atoms, in a $3\times3\times3$ supercell

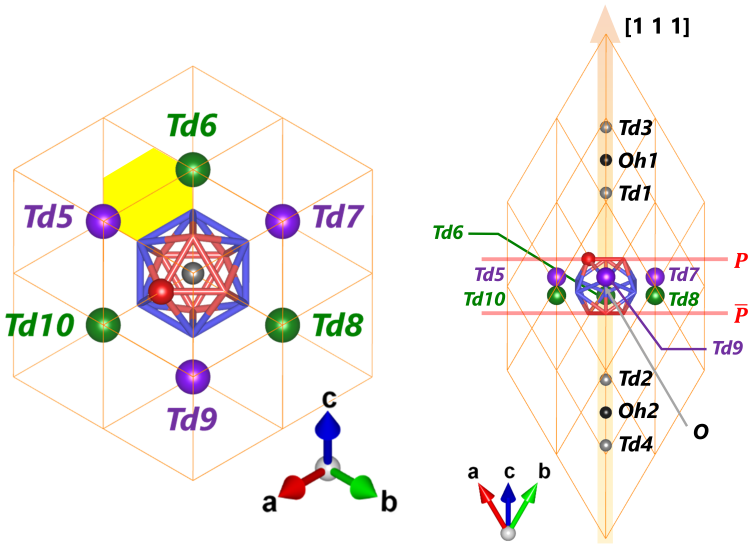

(a) (b)

Figure 1: (a) Atomic structure of $R\bar{3}m$ rhombohedral α boron used to model the carbon-based defects. View projected along the [111] rhombohedral axis. Orange solid lines enclose one primitive rhombohedral unit cell. While the calculations have been performed in 3×3×3 supercells, for clarity reasons we present the 2×2×2 excerption in the figure. Red (blue) edges: *polar* (*equatorial*) site that define a distorted (B_{12}) icosahedron. Grey ball: interstitial *Td* site along the [111] rhombohedral axis with tetrahedral symmetry. Green and violet balls: interstitial *Td* site not aligned with the [111] rhombohedral axis. When two carbon atoms are positioned in the *Td* sites of one violet ball and one neighboring green ball, e.g. *Td5* and *Td6*, they form a puckered hexagonal ring (yellow hexagon) with two boron atoms in the *equatorial* site of an icosahedron they have in common (the icosahedron at the center) and two boron atoms in the *equatorial* site of the other icosahedron they have in common (not shown). Red ball: intraicosahedral *p1* atomic position. (b) Grey (black) balls: interstitial *Td* (*Oh*) site along the [111] rhombohedral axis, with tetrahedral (octahedral) symmetry. Point *O* indicated with the grey arrow: center of the (B_{12}) icosahedron, that aligns with *Td1*–*Td4* and *Oh1*–*Oh2* along the [111] direction. The *P* plane is the (111) basal plane that contains three symmetry-equivalent *polar* atoms, including the *p1* atomic position (red ball in the icosahedron). The $\bar{P}$ plane is the (111) basal plane that contains three *polar* atoms and that is related to the *P* plane through the inversion symmetry w.r.t. the (empty) center of the icosahedron (*O*). ~~The *p1* and *p4* planes contain three symmetry-equivalent *polar* atoms and are related to each other through the inversion symmetry defined by the (empty) center of the icosahedron (*O*). Out of the [111] axis,~~ In panel (a), the *Td* sites form another puckered hexagon, with green (resp. violet) sites being above (below) the plane perpendicular to the [111] direction and passing through the (unoccupied) center of the icosahedron, *O*. The *equatorial* sites form a third puckered hexagon (blue hexagon), and this is due to the distortion of the icosahedron. All of the interstitial sites remain vacant in pristine α boron, while all of the *polar* and *equatorial* sites are occupied by boron atoms.

and studied all of the possible configurations with the insertion of one and two carbon atoms in the interstitial *Td* atomic sites of B_4C, both with

and/or without one substitutional carbon atom in the intraicosahedral *polar* site (figure 1). This leads to the following seven models (table 1, from top row to bottom row): one (B_{12}) icosahedron and respectively, two interstitial C atoms; two interstitial C and B atoms; three interstitial C and B atoms; alternatively, the atomic model consists in one ($B_{11}C$) icosahedron and, respectively, one single C interstitial atom; two interstitial C and B atoms; two interstitial C atoms; three interstitial C and B atoms. We note that the models with two substitutional atoms in the icosahedron turn out to be higher in energy by 1.1 eV/defect [26] and are not discussed further.

The atomic geometry is defined by three geometric parameters that depend on the relative positions of the carbon or boron atoms forming the defect. When two interstitial atoms sit in a plane perpendicular to the [111] direction passing through the center of the icosahedra they have in common, the angles that they form w.r.t. the icosahedron centers, $\angle C^{Td}OC^{Td'}$, are equal and form the main geometric characteristics, noted ~~$\angle C^{Td}OC^{Td'}$~~ γ in the following. This occurs when the atoms sit in two of the *Td5–Td10* positions (figure 1(a)). The in-plane configuration leads to the formation of puckered hexagons, in the same way as equatorial atoms of the same icosahedron form a puckered hexagon: the *Td5*, *Td7* and *Td9* atoms are in a plane slightly above the plane defined by the *Td6*, *Td8* and *Td10* positions (respectively violet and green balls). When, by contrast, the atoms are aligned along the [111] direction, the distance between two interstitial atoms is called the C^{Td}–$C^{Td'}$ distance and is the main geometric parameter when they sit in two of the *Td1* to *Td4* sites (figure 1(b)). Finally, when the icosahedron is changed from (B_{12}) to ($B_{11}C^{p}$), where p stands for the polar site of the icosahedron, the icosahedron center (O in figure 1(b)) is always chosen to be aligned with the eventual interstitial atoms along the [111] direction. The distance between the substitutional atom and an interstitial one is called the C^{p}–C^{Td} distance. The three geometric parameters will be discussed in the next section. Two last cases occur when one interstitial atom sits in a basal plane (*Td5–Td10*) while the second interstitial atom sits in one of the two closest *Td* positions along [111] (*Td1–Td4*). We call these configurations the *around 90 degree* ($\sim 90°$) configurations and we do not vary their geometric parameters.

In addition, defects with one carbon atom studied in Ref. [5] are presented in Appendix A. They are not discussed in the main text because the geometric parameters are not relevant for these defects.

We have also studied intericosahedral structures that appear in boron-rich boron carbides [4] as defective chains, which turned out to have higher values of the formation enthalpy than the configurations reported in table 1. They are discussed in Appendix B.

When there are two interstitial atoms in two *Td* sites along the [111] direction, the octahedral *Oh* site between the two *Td* sites may be vacant or not. We use the notation $C^{Td}\square C^{Td'}$, where the square symbol stands

for the vacancy, when the *Oh* site is vacant. Such cases are for instance configuration (config.) II of the $(B_{12})C^iC^j$ model, and configs. IV and V of the $(B_{11}C^{p1})C^iC^j$ model (table 1, brackets). When instead a carbon–carbon bond is present between two C^{Td} atoms, the notation is C^{Td}–$C^{Td'}$, as for config. III of the $(B_{12})C^iC^j$ model, and configs. I and II of the $(B_{11}C^{p1})C^iC^j$ model.

Configuration → / Model ↓	I	II	III	III′	III″	IV	V	VI	VII	VIII	IX
$(B_{12})C^iC^j$											
	$\perp$	$\parallel$	$\parallel$	$\sim 90°$	$\sim 90°$	$\parallel$	$\parallel$	$\parallel$	$\perp$	$\perp$	
i	$Td5$	$\langle Td1 \rangle$	$Td1$	$Td1$	$Td1$	$Td3$	$Td1$	$(Td1)$	$Td5$	$Td5$	
j	$Td6$	$\langle Td3 \rangle$	$Td3$	$Td5$	$Td6$	$Td4$	$Td4$	$(Td2)$	$Td7$	$Td8$	
$(B_{12})B^iC^j$											
	$\parallel$	$\parallel$									
i	$Td1$	$\langle Td1 \rangle$									
j	$Td3$	$\langle Td3 \rangle$									
$(B_{12})C^iB^{Oh1}C^j$											
	$\parallel$										
i	$Td1$										
j	$Td3$										
$(B_{11}C^{p1})C^i$											
	$\perp$	$\perp$	$\perp$			$\perp$					
i	$Td5$	$Td7$	$Td6$			$Td10$					
$(B_{11}C^{p1})C^i$											
	$\parallel$	$\parallel$	$\parallel$			$\parallel$					
i	$Td4$	$(Td2)$	$Td3$			$Td1$					
$(B_{11}C^{p1})B^iC^j$											
	$\parallel$	$\parallel$	$\parallel$			$\parallel$	$\parallel$	$\parallel$	$\parallel$		
i	$Td3$	$Td1$	$Td4$			$Td2$	$\langle Td2 \rangle$	$\langle Td4 \rangle$	$\langle Td1 \rangle$		
j	$Td1$	$Td3$	$Td2$			$Td4$	$\langle Td4 \rangle$	$\langle Td2 \rangle$	$\langle Td3 \rangle$		
$(B_{11}C^{p1})C^iC^j$											
	$\parallel$	$\parallel$	$\perp$			$\parallel$	$\parallel$	$\parallel$	$\parallel$	$\parallel$	$\parallel$
i	$Td2$	$Td1$	$Td5$			$\langle Td2 \rangle$	$\langle Td1 \rangle$	$Td3$	$Td2$	$Td1$	$(Td1)$
j	$Td4$	$Td3$	$Td6$			$\langle Td4 \rangle$	$\langle Td3 \rangle$	$Td4$	$Td3$	$Td4$	$(Td2)$
$(B_{11}C^{p1})C^iB^jC^k$											
	$\parallel$	$\parallel$	$\parallel$			$\parallel$					
i	$Td2$	$Td1$	$Td1$			$(Td1$					
j	$Oh2$	$Oh1$	$Td3$			$Td4$					
k	$Td4$	$Td3$	$Td2$			$Td2)$					

Table 1: Seven atomic models (bold font) for defects in α boron, with varying number of interstitial atoms from one to three with, from top to bottom, (B_{12}) and $(B_{11}C)$ icosahedra. Defect configurations I to IX are ordered by increasing formation enthalpy per defect. Each configuration is defined by the location of interstitial atom(s), labeled by i, j, and k indices as given in figure 1. When the C^{Td} atom - or both C^{Td} atoms if the model contains two of them - is positioned in a plane that is perpendicular to the [111] direction (green and violet balls in figure 1), the configuration is marked with the $\perp$ symbol and when positioned along the [111] direction (wide orange arrow in figure 1(b)), the configuration is marked with the $\parallel$ symbol. The $\sim 90°$ stands for the intermediate case which is explained in the main text. Configurations studied in Ref. [5] are given in parentheses. Configurations where a vacancy is present between two interstitials are given in brackets.

2.2. Computational details

Each of the defects described in the previous section has been introduced in a $N \times N \times N$ supercell of α boron where $N = 3$. Therefore, the supercell

consisted of 27 elementary rhombohedral unit cells. The total number of atoms ranged from 324 to 328.

The total energy, equilibrium volume, and band structure of pristine and defective systems have been computed using the DFT calculations, with the plane wave and pseudopotential method, in the generalized gradient approximation (GGA) with the PW91 functional (DFT-GGA-PW91) [27]. In the neutral charge state, the supercell volume and atomic positions have been fully relaxed, while in the charged state, the volume was fixed to that of the neutral state. The pseudopotentials for B and C atoms were identical to those of Ref. [28]. The plane wave energy cutoff has been set to 100 Ry for the size of the plane wave basis set. In order to compute metallic defects, calculations for all of the defects considered the spreading of the eigenvalues of 0.03 eV using the Methfessel–Paxton first-order spreading [29]. A 3^3 Monkhorst–Pack (MP) **k**-point mesh [30] has been used to sample the Brillouin zone (BZ) of the $3 \times 3 \times 3$ supercells. The density of the **k**-point meshes has been chosen from the unit cell calculations of α boron where 8^3 MP **k**-point mesh turned out to be well-converged within the error bar of 10^{-5} Ry in the total energy.

2.3. Calculation of the formation enthalpy

In this work we deal with various defects with different numbers of atoms and/or electrons, leading to different stoichiometries and charge states, respectively. To compare their stabilities, computations of the formation enthalpy of each defect have been done as follows [31, 32, 33, 34, 35, 24]:

$$\Delta H_{D,q}(\mu_e, \mu_m) = (E_{D,q} - E_H) + \sum_{m=B,C} n_m \mu_m + q(E_{VBM} + \mu_e) + \frac{q^2 \alpha_M}{2L\epsilon}, \quad (1)$$

$$\mu_m = \mu_m^0 + \mu_m^*, \quad (2)$$

$$0 \leq \mu_e \leq E_g \quad (3)$$

where D and q indicate the defect type and the charge state of the defect. $E_{D,q}$ and E_H are total energies of the defective system and host material, respectively, the host being in our case α boron. When positive, the value of the formation enthalpy informs us about the magnitude of the destabilization of the system by the defect, w.r.t. the pristine material. A contrario, a negative value indicates that the defect makes the system more stable than pristine α boron.

μ_m indicates the chemical potential of an atom of element m, being either B or C. n_m indicates the number of atoms of element m that are given to (positive) or supplied from (negative) one reservoir of B atoms and/or one reservoir of C atoms. The ideal chemical potentials μ_B^0 and μ_C^0 are taken from the total energy of pristine α boron and diamond, respectively: $\mu_B^0 =$

$E_{tot}(\alpha\text{-}B_{12})/12$ and $\mu_C^0 = E_{tot}(\text{diamond})/2$, where $E_{tot}(\alpha\text{-}B_{12})$ indicates the total energy of a 12-atom unit cell of pristine α boron and $E_{tot}(\text{diamond})$ indicates the total energy of a 2-atom unit cell of diamond. The excess chemical potentials μ_B^* and μ_C^* define the chemical environment and have been computed from the formation energy of B_4C boron carbide [36, 5]. In the following, the chemical environment is fixed to the boron-rich limit ($\mu_B^* = 0$) unless otherwise stated, and the carbon-rich limit ($\mu_C^* = 0$) is reported in Appendices.

When the defect is charge neutral ($q = 0$), Eq. 1 is a function of μ_B and μ_C. When the defect is positively or negatively charged, another parameter comes into play in Eq. 1: The electronic chemical potential, μ_e. It is set to zero at the valence band maximum, which is indicated by E_{VBM}. E_{VBM} has been computed as in Ref. [5]. The upper limit of μ_e is its value at the conduction band minimum, E_{CBM}, which corresponds to the band gap, E_g. The last term accounts for the correction of spurious interactions within periodic array of additional charges, which occurs from the periodic boundary condition. L corresponds to the cubic root of the volume of computed supercell.

2.4. Calculation of defect charge states

Charged defects have been computed while the supercell volume was fixed to the equilibrium volume of the defect neutral state [38] (defect atomic volume [39] are reported in Appendices, in particular in table C.4). Meanwhile, the atomic positions were relaxed. Defects that contain a substitutional and/or interstitial site that breaks the rotational symmetry w.r.t. the [111] rhombohedral axis, *e.g.* colored balls in figure 1, break the rhombohedral symmetry. For instance, a ($B_{11}C^p$) icosahedron lowers the symmety from rhombohedral to monoclinic. We note that all of the charged defects have been computed in the supercell with rhombohedral symmetry. In the case where the neutral defect has a symmetry lower than the rhombohedral one, the lattice parameters have been averaged to give a rhombohedral supercell with the quasi-identical volume. We have checked that the resulting error in total energy is kept below 0.65 meV/unit cell.

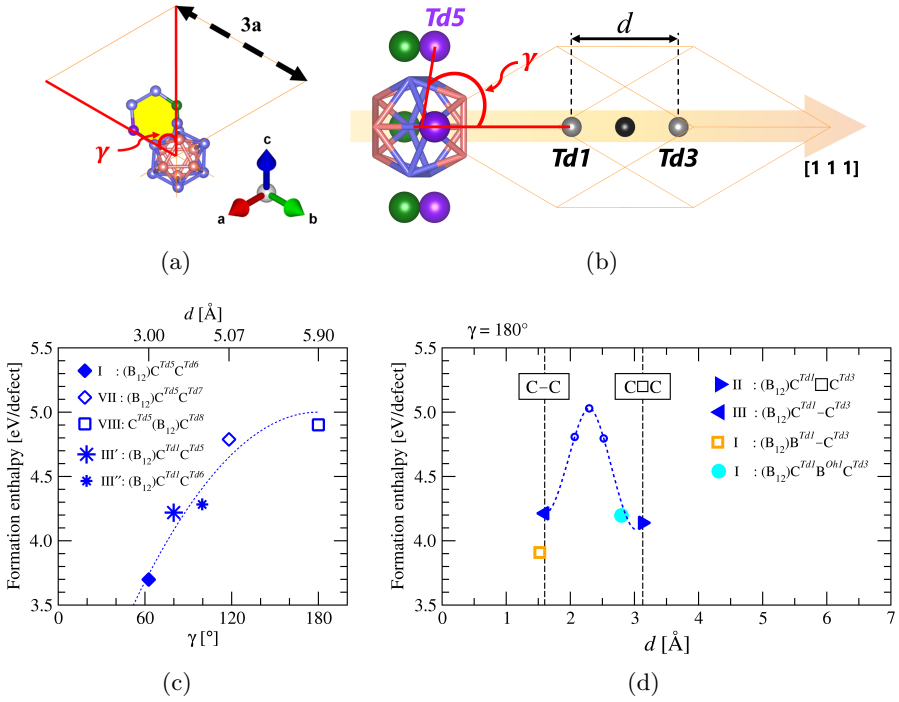

Figure 2: (a) Same as figure 1(a) with two carbon atoms (green and violet balls) from configuration I of the $(B_{12})C^iC^j$ model. Visualized in a $3 \times 3 \times 3$ supercell (indicated as 3a) and the formed B_4C_2 puckered hexagon indicated in yellow. Red (blue) balls: *polar* (*equatorial*) boron atoms. Violet (green) ball: carbon atom in the *Td5* (*Td6*) atomic position. The angle γ stands for the angle $\angle C^{Td}OC^{Td'}$ formed by the C^{Td} atom, the center of the icosahedron (O), and the $C^{Td'}$ atom. (b) Same as figure 1(b) with the definition of the distance d and the angle γ. Formation enthalpy of the $(B_{12})C^iC^j$ (blue symbols), $(B_{12})B^iC^j$ (orange square) and $(B_{12})C^iB^jC^k$ (light blue disk) models as a function of (c) ~~the angle formed by the C^{Td} atom, the center of the icosahedron (O), and the $C^{Td'}$ atom, indicated as $\angle C^{Td}OC^{Td'}$~~γ, when the two C atoms are out of the [111] direction or in the $\sim 90°$ configurations (blue stars); (d) the distance between the two ~~carbon~~ atoms in the *Td* site when they are along the [111] direction. In panel (c), the alternate abscissa axis on top indicates the distance between two carbon atoms in-plane. For the $\sim 90°$ configurations, $d = 5.04$ and 5.89 Å while the formation enthalpy differs by 64 meV/defect. ~~Inset in panel (a): config. I visualized in a $3 \times 3 \times 3$ supercell (indicated as 3a) and the formed B_4C_2 hexagon indicated in yellow.~~ Blue dotted curve in panel (c): polynomial fit of the formation enthalpy as a function of ~~$\angle C^{Td}OC^{Td'}$~~γ from the configurations of the $(B_{12})C^iC^j$ model that are marked with the $\perp$ symbol in table 1 [37]. Empty blue circles in panel (d): non-equilibrium configurations where the distance between two carbon atoms has been fixed and the energy barrier computed. The blue dotted curve is a guide for the eye. In configurations I–III, two atoms in the *Td* site are not screened by a (B_{12}) icosahedron between them.

3. Effect of the defect atomic geometry on the formation enthalpy

In the present section, we study neutral configurations with more than one carbon atom per defect, and report results for the formation enthalpy

at the B-rich limit only ($\mu_B^* = 0$).

3.1. Atomic models with interstitial carbon and boron atoms

We first fix the icosahedron to (B_{12}) and study defect configurations that consist of two interstitial atoms in two *Td* sites, either with or without a boron atom in the *Oh* site that is in between (table 1, rows for the first, second, and third atomic models). Results are given in figure 2, as a function of the angle between the two C^{Td} atoms and the center of each of the two icosahedra they have in common, when the two carbon atoms are in a plane (quasi) perpendicular to the [111] direction. Or they are given as a function of the distance along the [111] direction.

We discuss the ~~five~~ configurations that have the lowest formation enthalpy values that come from three different atomic models (table 1). The smallest formation enthalpy value is reached for config. I of the first model, $(B_{12})C^{Td5}C^{Td6}$, 3.70 eV/defect, with two nearby carbon atoms in a plane quasi-perpendicular to the [111] direction (figure 2(c), filled diamond). As the first point of extreme importance, this corresponds to the formation of a puckered B_4C_2 hexagon in-plane with four equatorial atoms (figure 2(c), inset).

Then come: config. I of the second model, $(B_{12})B^{Td1}$–C^{Td3}, 3.91 eV/defect, where one interstitial boron atom and one interstitial carbon atom form a bond between them (orange square); config. II of the first model, $(B_{12})C^{Td1}\square C^{Td3}$, 4.14 eV/defect, where the two carbon atoms are aligned along the [111] direction and have a vacant *Oh* site between them (right filled triangle); config. I of the third model, $(B_{12})C^{Td1}B^{Oh1}C^{Td3}$, 4.20 eV/defect, which has a chain that is analogous to that of B_4C boron carbide [21, 40, 41, 28] (light blue disk); config. III of the first model, $(B_{12})C^{Td1}$–C^{Td3}, 4.21 eV/defect, where the two carbon atoms form a bond (left filled triangle). The C–B–C chain is thus very close in energy to C□C and C–C (config. II and III). Finally, the formation enthalpy of the two $\sim 90°$ configurations, 4.22 eV/defect or 4.28 eV/defect (config. III′ and III″, respectively), are close to that of the C–C defect (config. III), and nicely agrees with the angle dependence of in-plane defects: the blue star symbols in figure 2(c) are close to the dotted line. We will see below that the energetics is modified when the icosahedron is ($B_{11}C^p$) instead of (B_{12}).

Going from $C^{Td1}\square C^{Td3}$ (config. II) to C^{Td1}–C^{Td3} (config. III), the C^{Td}–$C^{Td'}$ distance is halved from 3.1 Å to 1.6 Å, and the energy barrier height is around 0.9 eV (empty blue circles and dotted line). Such a barrier has also been found in boron carbide [42, 43] with however the energy barrier value smaller by one-third (0.3 eV) at 0 GPa [43]. The equilibrium volumes of configs. II and III of the first model are reported in Appendix C, as well as those of the other defects. As the second extremely important point, we will see in Section 4 that charging config. II with two electrons makes the presence of a vacancy unstable, and leads to a defect similar to config. III.

Remaining configurations of the $(B_{12})C^iC^j$ and $(B_{12})B^iC^j$ atomic models are discussed in Appendix D.1. Configs. IV–VI of the $(B_{12})C^iC^j$ model have formation enthalpy values that are close to twice the value of the isolated $(B_{12})C^{Td}$ defect, so that no energy gain is obtained from the formation of such complex defects.

In summary, we find that the in-plane configuration with two first neighbor atoms has the lowest formation enthalpy. It is followed by the B–C chain. Then, the C□C, C–B–C, and C–C chains along the [111] direction have the same formation enthalpy within 70 meV/defect. Then they are followed by the $\sim 90^\circ$ configs. III′ and III″ that have the formation enthalpy 5–69 meV/defect higher than that of the C–C chain.

3.2. Changing the (B_{12}) icosahedron to ($B_{11}C^p$)

We now turn to defects with a $(B_{11}C^p)$ icosahedron rather than a (B_{12}) icosahedron and discuss the rows for models 4 to 7 (table 1). We fix the *polar* carbon atoms at position p=*p1* (figure 1, red ball).

3.2.1. Atomic models with one interstitial carbon atom

The configurations of the $(B_{11}C^p)C^i$ model (table 1, fourth model) have the lowest formation enthalpy values among all of the interstitial defects that also contain a substitutional C^p atom. When the interstitial atom sits in-plane at one of the *Td5* to *Td10* positions (figure 1(a)), the formation enthalpy ranges between 4.15 and 4.34 eV/defect. When the interstitial carbon atom is positioned at one of the *Td1*–*Td4* tetrahedral sites (figure 1(b)), the formation enthalpy turns out to be ≈ 4.55 eV/defect within a configuration-dependent fluctuation of ± 20 meV/defect. We find almost no effect of the C^p–C^{Td} distance on the defect formation enthalpy (Appendix E).

3.2.2. Atomic models with two or three interstitial atoms

In the present section, we study defects that contain two (table 1, fifth and sixth models) or three (table 1, seventh model) interstitial atoms. Like in Section 3.1, we limit the discussion to ~~discuss~~ the ~~five~~ configurations that have the lowest formation enthalpy values. We have five such configurations.

The $(B_{11}C^p)B^iC^j$ model has the lowest formation enthalpy values when a bond forms between two interstitial atoms, irrespective of the occupation of the (*Td1*,*Td3*) and (*Td2*,*Td4*) site pairs. The average value is 5.01 ± 0.15 eV/defect (figure 3(b), light green symbols) and the B^{Td}–$C^{Td'}$ distance is 1.57 Å.

The second smallest formation enthalpy value, 5.22 eV/defect, is given by the $(B_{11}C^p)C^iC^j$ model, with the C^{Td}–$C^{Td'}$ bond formed between the interstitial carbon atoms (configs. I and II, dark green point and empty diamond symbol). We discuss the effect of the C^{Td}–$C^{Td'}$ distance in Appendix D.2, and the effect of the C^p–C^{Td} distance in Appendix E.

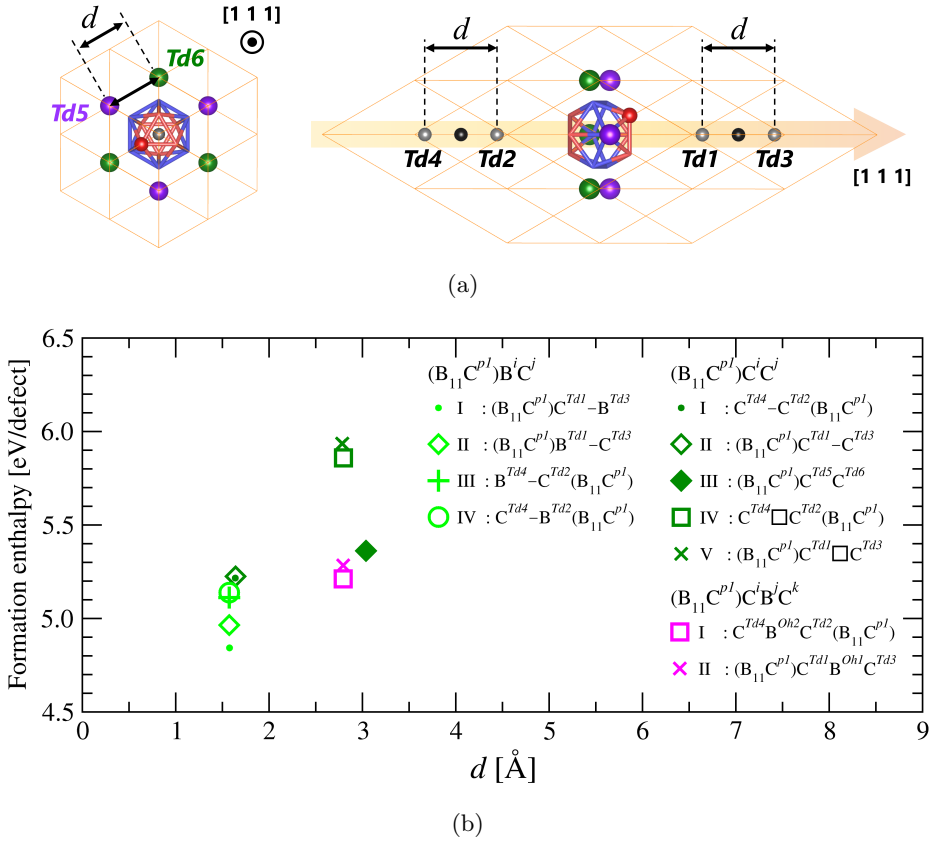

Figure 3: (a) Same as figure 1 with the definition of *d*. (b) Formation enthalpy of the $(B_{11}C^{p1})B^iC^j$ (light green symbols), $(B_{11}C^{p1})C^iC^j$ (dark green symbols) and $(B_{11}C^{p1})C^iB^jC^k$ (magenta symbols) models as a function of ~~the distance between the two C^{Td} atoms~~*d*.

As the third extremely important point, the formation of a C^{Td}–B^{Oh}–$C^{Td'}$ chain (table 1, seventh model, configs. I and II) gives similar formation enthalpy value, 5.25 eV/defect (magenta square and cross symbols), to the configurations with the C^{Td}–$C^{Td'}$ bond (dark green point and empty diamond symbol). We remind the reader that such C–B–C chains are the main components in the intericosahedral space of B_4C boron carbide.

Config. III of the $(B_{11}C^p)C^iC^j$ model (table 1, sixth model) has the next smallest formation enthalpy, 5.36 eV/defect. This is the case where two C^{Td} atoms are in a plane that is quasi-perpendicular to the [111] direction and form the puckered B_4C_2 hexagon also reported in Section 3.1.

The fifth smallest formation enthalpy value, 5.90±0.04 eV/defect, comes from the C^{Td}□$C^{Td'}$ case (configs. IV and V, table 1, fifth model), where two interstitial carbon atoms are aligned along the [111] direction with a vacant *Oh* site between them (dark green square and cross symbols).

Remaining configs. V–VII of the $(B_{11}C^p)B^iC^j$, VI–IX of the $(B_{11}C^p)C^iC^j$, and III–IV of the $(B_{11}C^p)C^iB^jC^k$ models are reported in Appendix D.2 and Appendix E.

In summary, when the icosahedron is $(B_{11}C^p)$, and apart from the $(B_{11}C^p)$ itself (Appendix A), the defect formation enthalpy is somewhat higher than the case where it is (B_{12}), so that the formation of a defect is less probable under thermodynamical conditions. We find that all of the B–C chain configurations have the lowest formation enthalpy values when the defect icosahedron contains one susbtitutional *polar* carbon atom. They are followed by energetically quasi-equivalent C–C chain, C–B–C chain, and the in-plane configuration with puckered B_4C_2 hexagon. Higher in energy comes the C□C case.

3.3. Conclusions on neutral defects

Computation of the formation enthalpy values of neutral defects enables us to conclude that the atomic geometry of carbon-based defects in the atomic structure of α boron plays an important role in the formation enthalpy when the defect contains two or more interstitial atoms. The key factors are *(i)* the angle with which a puckered B_4C_2 hexagon starts to form in the basal plane, or the $\sim 90^\circ$ angle when one C^{Td} atom sits in-plane and one C^{Td} atom sits along [111]; *(ii)* the distance between interstitial carbon atoms when they are aligned along the [111] direction. On the other hand, both distance between substitutional and interstitial carbon atoms and the angle that they form with the center of the icosahedron play only a minor role in the formation enthalpy (Appendix E).

When the icosahedron is (B_{12}), low-energy neutral defect is $(B_{12})C^{Td}$. For higher carbon concentrations, the five most stable model configurations with two or three interstitial atoms are the puckered B_4C_2 hexagon in-plane, similar to graphene. Then come: the B–C chain, the C□C *Oh* vacancy case, the C–B–C and C–C chains, and the two $\sim 90^\circ$ configurations, by order of increasing formation enthalpy. Changing the defect icosahedron from (B_{12}) to $(B_{11}C^p)$ increases the formation enthalpy by approximately 1.14 eV/defect. The low energy models are preserved but the order is different: the B–C, C–C, C–B–C chains, the puckered B_4C_2 hexagon, and the C□C *Oh* vacancy case. This allows us to predict the atomic structure of carbon-defects in α boron when the carbon concentration is high enough.

Finally, the carbon-based defects that have the lowest formation enthalpy values are the one-carbon-atom defects with formation enthalpy values of 2.25 eV/defect $[(B_{12})C^{Td}]$; 2.73 eV/defect $[(B_{11}C^p)]$; and 3.77 eV/defect $[(B_{11}C^e)]$.

4. Results on the formation enthalpy of charged defects

In the present section, our aim is to determine the charged state of the defects studied in Section 3. To this end, we report the formation enthalpy as a function of the electronic chemical potential (see Eq. 1). In the following, we discuss only the three defects having the lowest energy. The study of the other defects as well at the C-rich limit are reported in Appendix F.

The lowest formation enthalpy values for one single carbon-based defects $(B_{12})C^{Td}$ and $(B_{11}C^{p})$ are found for the charge state of $q = -1$ and $q = +1$, respectively (figure 4(a), blue and black curves). This was found in Ref. [5] with a $2 \times 2 \times 2$ supercell modeling, and is confirmed here for a $3 \times 3 \times 3$ supercell.

Remarkably, we find that when charged, config. II of the $(B_{12})C^{i}C^{j}$ model that was initially $(B_{12})C^{Td1}\square C^{Td3}$ shows a drastic decrease in the formation enthalpy (red dotted line). In fact, it is no longer *stable* in the sense that the *Oh* site is not vacant any longer when the charge state is $q = -2$: there is a transition between config. II and config. III upon charging the defect negatively. Such a transition has been reported in boron carbide, for which the mechanism was the application of pressure. The boron vacancy at the *Oh* site in B_4C boron carbide, C–□–C, transforms into a compacted C–C bond under pressure [36].
In our calculations however, the volume after charging is that of the neutral state of config. II. The C^{Td1}–C^{Td3} distance is found to relax from 3.1 Å ($q = 0$) to 1.7 Å ($q = -2$), forming the C^{Td1}–C^{Td3} bond. Interestingly, the formation enthalpy of the $(B_{12})C^{Td1}$–C^{Td3} with charge $q = -2$ is lower, within the accuracy of our calculations, than that of the $(B_{12})C^{Td}$ defect with $q = -1$ that was thought so far to be the defect of lowest formation enthalpy [5]. Indeed, at the bottom of the conduction band, its formation enthalpy is as low as 0.46 eV/defect (figure 4(a), red dotted curve). Looking at the C-rich limit, the formation enthalpy even becomes negative w.r.t. pristine α boron (see Appendix F). Variation of the electronic potential that shows this inspiring decrease in formation enthalpy can be carried out either by doping or by electrostatic gating [44].

We now report the formation enthalpy as a function of the charge state (figure 4(b)), for three values of the electronic chemical potential: close to the VBM ($\mu_e = 0$), at mid-gap ($\mu_e = 1.3$ eV), and close to the CBM ($\mu_e = 2.25$ eV) [45]. Near the VBM, the positively charged $(B_{11}C^{p})$ has the lowest formation enthalpy (1.01 eV/defect). The doubly-positively charged state is also close (1.32 eV/defect). In wide contrast, there are four defects that compete at mid-gap ($\mu_e = 1.3$ eV) as they have very close formation enthalpy values: the positively charged $(B_{11}C^{p})$, the neutral $(B_{12})C^{Td}$, the negatively charged $(B_{12})C^{Td}$, and the doubly-negatively charged $(B_{12})C^{Td1}$–C^{Td3}. Their formation enthalpy values are in the range of 2.37±0.12 eV/defect. At $\mu_e = 2.25$ eV (CBM), the most stable defect is the doubly-negatively

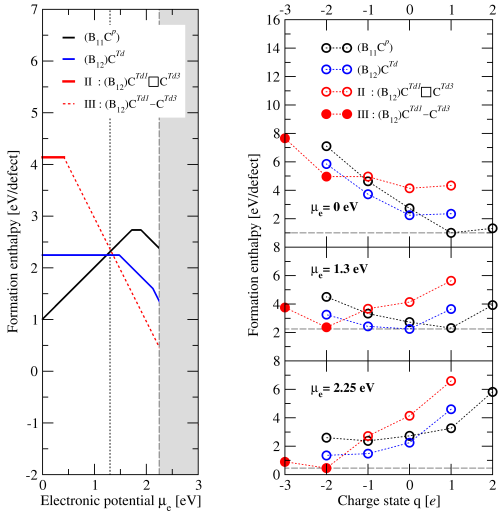

(a) (b)

Figure 4: Formation enthalpy of the defects that have the lowest values: $(B_{11}C^p)$, $(B_{12})C^{Td}$, and configurations II and III of the $(B_{12})C^iC^j$ atomic model (table 1, first model). (a) Formation enthalpy as a function of the electronic chemical potential [45]. (b) Formation enthalpy as a function of the charge state. The electronic chemical potential is fixed at 0 eV, 1.3 eV, and 2.25 eV (from top to bottom) of which the latter two μ_e values are indicated by dotted and dashed vertical lines in panel (a). Note that the volume of the charged config. III is that of the neutral state of config. II and amounts to 7.34 Å^3/atom, while the volume of the neutral state of config. III is 7.30 Å^3/atom (table C.4).

charged $(B_{12})C^{Td1}$–C^{Td3}.

In conclusion, additional charge enables transition between different configurations of a two-carbon-atom defect and can lower the formation enthalpy to an extent where it becomes more stable than the single-carbon-atom defect.

5. Conclusions

Extensive calculations of the low energy defects in α boron have been performed within the density functional theory framework, and has enabled us to propose a classification of the configurations of carbon-based defects.

We find that the atomic geometries of defects that contain two or more impurity atoms - substitutional carbon, interstitial carbon, and interstitial boron - affect the stability. Three conclusive rules have been derived from the inspection of defect formation enthalpy values with varying geometry: *i)* when two or more interstitial atoms exist in-plane, they preferentially form a puckered B_4C_2 hexagon, leading to graphite-like configurations for the carbon impurities, *ii)* when two or more interstitial atoms exist along the [111] rhombohedral axis, the distance between the interstitial atoms controls

the thermodynamic stability of defect, *iii)* one substitutional carbon atom in the icosahedron overall increases the defect formation enthalpy, but the C^p–C^{Td} distance and angles that include C^p do not play a big role.

The formation enthalpy values of various geometries of carbon-based defects in α boron have brought us the consensus that five diatomic or triatomic interstitial defects are close in energy. Those are: the puckered B_4C_2 hexagon; the B–C and C–C chains in which atoms are bonded in the chains; the C□C case where no bond is formed; and the C–B–C triatomic chain. When there is no substitutional carbon atom, the five interstitial defects are ordered by increasing formation enthalpy as given above, except for the C–C chain, which has the highest value and is close to the $\sim 90^\circ$ configurations. When there is one substitutional carbon atom within the icosahedron, there is a change in the ordering: the most stable interstitial defect is the bonded B–C chain; then comes the C–C and C–B–C chains, as well as the puckered B_4C_2 hexagon, that are close in energy within 150 meV/defect. The C□C is the least stable defect and is distant from the C–C and C–B–C chains by 0.6–0.7 eV/defect, in contrast to the case with no substitutional carbon atom, where the three defects are close in energy.

Interestingly, additional charges turned out to drastically modify the relative stability of the interstitial defects. With two additional electrons, the formation of a C–C bond greatly lowers the formation enthalpy, which makes this defect the most probable - together with the ($B_{11}C^p$) - among the defects that we have studied so far. This study allows the understanding of the mechanism of formation of carbon-defects in α boron with increased carbon concentrations, that paves a way to the design of carbon-based spin defects in icosahedral boron.

6. Acknowledgement

Calculations have been performed with the Quantum ESPRESSO suite of softwares [46]. This work has been granted access to HPC resources by the French HPC centers GENCI-IDRIS, GENCI-CINES and GENCI-TGCC (Project 2210) and by the École Polytechnique through the 3Lab cluster, and, at an early stage of the project, by the Partnership for Advanced Computing in Europe (PRACE Project No. 2019204962). We acknowledge support from the ANR BCSi and SADAPTH projects. The PhD fellowship of Y. Cho has been provided by the École Doctorale of the Institut Polytechnique de Paris via the ANR-21-CMAQ-002 project.

Appendix A. Defects with one single carbon atom

Defects containing one single carbon atom have been studied in Ref. [5] in a $2 \times 2 \times 2$ supercell, and are reported in the present work for a $3 \times 3 \times 3$ supercell. The two main carbon-based defects that turned out to have the

lowest formation enthalpy are the insertion of a carbon atom at the *Td* interstitial site (figure 1(b)), leading to the $(B_{12})C^{Td}$ defect [5] (figure 5(a)); and the substitution of a boron atom by a carbon atom in one of the six equivalent atomic positions of the *polar* site of the icosahedron (red corners of icosahedron in figure 1(b)), leading to the $(B_{11}C^{p})$ defect (figure 5(b)). The carbon substitution in the *equatorial* site, the $(B_{11}C^{e})$ defect (figure 5(c)), has a somewhat higher formation enthalpy [5].

In the main text, we demonstrate that the insertion of multiple C^{Td} atoms would occur by planar distribution while the characteristic angle ($\measuredangle C^{Td}\!-\!\!\!\!\!O\!\!\!\!\!-\!C^{Td'}$ γ) plays an important role (Section 3.1). Finally, the interstitial site with octahedral symmetry, *Oh*, turns out to be an unstable position for the insertion of a carbon atom.

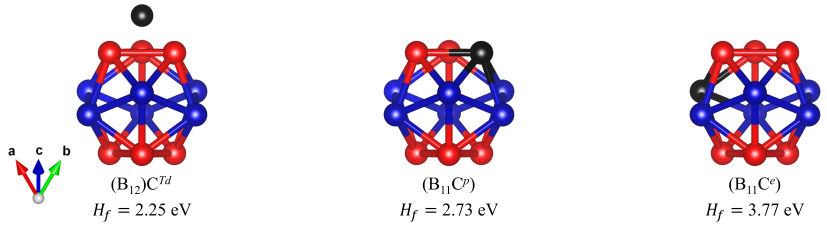

(a) (b) (c)

Figure 5: The atomic structure and formation enthalpy value of the simplest carbon-based defects in α boron when one single carbon atom is inserted in the $3 \times 3 \times 3$ supercell of α boron, ordered by increasing formation enthalpy: (a) $(B_{12})C^{Td}$; (b) $(B_{11}C^{p})$; and (c) $(B_{11}C^{e})$. Red (blue) balls: boron atoms in the *polar* (*equatorial*) site of an icosahedron. Black balls: carbon atoms. The formation enthalpy values are defined at the B-rich limit ($\mu_B^* = 0$).

Defect	at. C (%)	H_f^C (eV/defect)	H_f^B (eV/defect)	V (Å^3/at.)	Δ_V (%)
α boron (Ref.)	0	0	0	7.29	0
Single-atom interstitial					
$(B_{12})C^{Td}$	0.31	1.51	2.25	7.32	+0.34
One substitutional C atom					
$(B_{11}C^{p})$	0.31	1.81	2.73	7.29	−0.08
$(B_{11}C^{e})$	0.31	2.85	3.77	7.30	+0.06

Table A.2: Single carbon-atom defects depicted in figure 5. Carbon concentration, formation enthalpy at the C-rich ($\mu_C^* = 0$) and B-rich ($\mu_B^* = 0$) limit H_f^C (H_f^B), atomic volume V, and defect-induced volume change Δ_V w.r.t. pristine α boron. The electronic potential was fixed to $\mu_e = 0$ in the defect formation enthalpy.

Appendix B. Intericosahedral motifs found in boron-rich boron carbides

Some of the intericosahedral structures in phases of boron carbide other than B_4C (i.e., in boron-rich phases) appear as ordered four-atom B–C–B–C chains or as $C\langle^{B}_{B}\rangle C$ or $B\langle^{B}_{B}\rangle B$ pantographs [47, 28, 2, 3, 4]. In α boron, they turn out to have formation enthalpy values ranging from 7.6 eV/defect to 9.1 eV/defect (at the B-rich limit), while all of the two-atom or three-atom interstitial defects have formation enthalpy below 6.1 eV/defect (table C.4). We conclude that these motifs have a small probability to occur as point defects in α boron.

Defect	at. C (%)	C^{Td}–$C^{Td'}$ distance (Å)	H_f^C (eV/defect)	H_f^B (eV/defect)	V (Å^3/at.)	Δ_V (%)	Parent phase
$B\langle^{B}_{B}\rangle B$ pantograph	0		9.84	9.10	7.33	+0.52	OPO1
B–C–B–C chain	0.61	2.77	6.51	7.62	7.32	+0.39	OPO2
$C\langle^{B}_{B}\rangle C$ pantograph	0.61	2.57	7.66	8.78	7.30	+0.14	OPO3

Table B.3: Intericosahedral chains found in boron-rich phases of boron carbide, OPO1–3 [4], taken as point defects in α boron. Carbon concentration, C–C distance, formation enthalpy at the C-rich (B-rich) limit H_f^C (H_f^B), atomic volume V, and defect-induced volume change Δ_V w.r.t. pristine α boron. The electronic potential was fixed to $\mu_e = 0$ in the calculation of the defect formation enthalpy.

Appendix C. Defect-induced volume change

In the present section, the equilibrium volume of neutral defects is studied and the change with respect to the volume of pristine α boron is analyzed (table C.4).

When the icoshedron is (B_{12}), a volume expansion has been found for all of the defects, with one exception: a volume contraction has been found for the single carbon atom substitution in the polar site $B_{11}C^p$ (Appendix A), which confirms for the $3 \times 3 \times 3$ supercell the contraction already reported for the $2 \times 2 \times 2$ supercell and observed in the experiments [5].

In addition, a quasi-stability of the volume is found for the single carbon atom substitution in the polar equatorial site $B_{11}C^e$ (Appendix A), and for the diatomic C–C chain, config. III of the $(B_{12})C^iC^j$ model (table 1, first model & table C.4, line 4).

When the icosahedron is ($B_{11}C^p$), a volume expansion has been systematically found except in the six cases where the chain is diatomic, for which a volume quasi-stability has been computed: the B–C chains, B^{Td2}–C^{Td4}, C^{Td2}–B^{Td4}, B^{Td1}–C^{Td3}, and C^{Td1}–B^{Td3} (table 1, sixth model, configs. I–IV & table C.4, lines 17–20); and the C–C chains, C^{Td2}–C^{Td4} and C^{Td1}–C^{Td3} (table 1, fifth model, configs. I–II & table C.4, lines 24–25).

Model	at. C (%)	Config.	Interatomic distance (Å) p–Td	p–Td'	Td–Td'	H_f^C (eV/defect)	H_f^B	V (Å^3/at.)	Δ_V (%)
α boron (Ref.)	0					0	0	7.29	0
Two-atom interstitial									
$(B_{12})C^{Td}C^{Td'}$	0.61	I			3.00	2.22	3.70	7.34	+0.61
		II			3.13	2.66	4.14	7.34	+0.67
		III			1.60	2.73	4.21	7.30	+0.04
		III′			5.04	2.74	4.22	7.34	+0.67
		III″			5.89	2.80	4.28	7.34	+0.67
		IV			15.73	2.84	4.32	7.34	+0.67
		V			12.55	2.99	4.47	7.34	+0.68
		VI			9.31	3.10	4.58	7.34	+0.67
		VII			5.07	3.31	4.79	7.35	+0.70
		VIII			5.90	3.42	4.90	7.34	+0.66
$(B_{12})B^{Td}C^{Td'}$	0.31	I			1.52	3.35	3.91	7.30	+0.15
		II			2.97	5.50	6.05	7.35	+0.75
Three-atom interstitial									
$(B_{12})C^{Td}B^{Oh1}C^{Td'}$	0.61	I			2.79	2.90	4.20	7.33	+0.44
One substitutional C atom & Single-atom interstitial									
$(B_{11}C^{p})C^{Td}$	0.62	I(⊥)	2.74			2.49	4.15	7.31	+0.19
		II(⊥)	4.00			2.53	4.19	7.31	+0.20
		III(⊥)	4.00			2.62	4.28	7.31	+0.20
		IV(⊥)	2.75			2.67	4.34	7.31	+0.20
		I(‖)	9.13			2.86	4.53	7.31	+0.20
		II(‖)	6.17			2.87	4.54	7.31	+0.20
		III(‖)	6.48			2.88	4.54	7.31	+0.20
		IV(‖)	3.57			2.90	4.56	7.31	+0.19
One substitutional C atom & Two-atom interstitial									
$(B_{11}C^{p})B^{Td}C^{Td'}$	0.61	I	5.56	4.01	1.58	3.36	4.84	7.30	+0.07
		II	4.39	5.95	1.57	3.48	4.96	7.30	+0.07
		III	8.21	6.64	1.57	3.63	5.11	7.30	+0.06
		IV	7.04	8.61	1.57	3.66	5.14	7.30	+0.06
		V	6.19	9.16	3.00	5.69	7.17	7.35	+0.72
		VI	9.06	6.09	3.00	5.71	7.20	7.35	+0.72
		VII	3.58	6.50	2.98	5.73	7.21	7.35	+0.70
$(B_{11}C^{p})C^{Td}C^{Td'}$	0.92	I	6.80	8.42	1.64	2.81	5.22(1)	7.29	+0.00
		II	4.16	5.77	1.64	2.82	5.22	7.29	−0.01
		III	2.81	4.02	3.04	2.95	5.36	7.33	+0.47
		IV	6.24	9.01	2.80	3.45	5.86	7.33	+0.48
		V	3.63	6.35	2.78	3.53	5.93	7.33	+0.47
		V′	3.50	4.03	4.98	3.73	6.14	7.33	+0.54
		V″	3.45	2.77	4.98	3.74	6.15	7.33	+0.52
		V‴	3.48	4.01	5.93	3.95	6.36	7.33	+0.54
		V⁗	3.44	2.73	5.96	4.03	6.43	7.33	+0.54
		VI	6.54	9.19	15.60	4.07	6.47	7.33	+0.53
		VII	6.12	6.58	12.54	4.20	6.61	7.33	+0.55
		VIII	3.52	9.25	12.56	4.26	6.66	7.33	+0.54
		IX	3.52	6.12	9.41	4.46	6.87	7.33	+0.53
One substitutional C atom & Three-atom interstitial									
$(B_{11}C^{p})C^{Td}B^{j}C^{Td'}$	0.92	I	6.26	9.03	2.80	2.99	5.21	7.33	+0.43
		II	3.65	6.39	2.79	3.06	5.28	7.32	+0.42
		III	4.03	6.07	9.90	5.31	7.53	7.32	+0.38
		IV	3.46	6.67	9.90	5.46	7.68	7.32	+0.38

Table C.4: Atomic models, their carbon concentration and configurations as described in table 1, the C–C distance(s), formation enthalpy at the C-rich (B-rich) limit H_f^C (H_f^B), atomic volume V, and defect-induced volume change Δ_V w.r.t. pristine α boron. The electronic potential was fixed to $\mu_e = 0$ in the defect formation enthalpy. When possible, the names of the sites $p/Td/Oh$ have been directly inserted into the model name instead of using the i, j, and k indices of table 1.

Appendix D. High formation enthalpy neutral defects

Appendix D.1. Neutral defects with two interstitial atoms

In the present section, the formation enthalpy of neutral defects with two interstitial atoms that have values larger or close to twice the isolated tetrahedral interstitial carbon atom is discussed. We generalize the distance and angle of the main text as follows: d^* is the distance between C^{Td} and C^{Td^*} atoms, where C^{Td^*} is defined as a $C^{Td'}$ atom in the neighboring supercell that makes the smallest C–C distance and that does not align with the C^{Td} atom along the [111] direction; γ^* is the angle $\angle C^{Td}OC^{Td^*}$ that two atoms, C^{Td} and C^{Td^*} from neighboring cells, form with the center of one of the two icosahedra that they share.

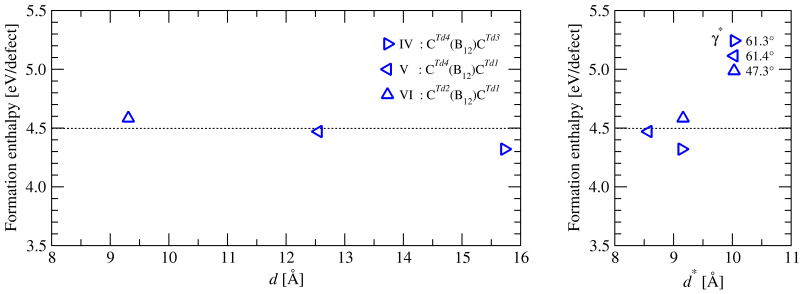

(a) (b)

Figure 6: Formation enthalpy of the $(B_{12})C^iC^j$ model as a function of (a) the distance between C^{Td} and $C^{Td'}$ atoms that are along the [111] direction, d; (b) the distance between C^{Td} and C^{Td^*} atoms, d^* ~~where C^{Td^*} is defined as a $C^{Td'}$ atom in the neighboring supercell that makes the smallest C–C distance and that does not align with the C^{Td} atom along the [111] direction~~. The characterized angle ~~$\angle C^{Td}OC^{Td^*}$ in each defect is shown in the legend.~~ γ^* is shown in the legend. Dotted line: the value of twice the formation enthalpy of the $(B_{12})C^{Td}$ defect.

Interstitial atoms in configs. IV–VI of the $(B_{12})C^iC^j$ model are located along the [111] direction. They have a formation enthalpy value equivalent to two isolated $(B_{12})C^{Td}$ defect (figure 6, dotted line), from which we conclude that the two carbon atoms behave as two isolated C^{Td} atoms along the [111] direction. Consequently the formation enthalpy only weakly varies with the C^{Td}–$C^{Td'}$ distance.

When one of the interstitial atoms is boron instead of carbon, the two configurations of the $(B_{12})B^iC^j$ model greatly differ in formation enthalpy, as $B^{Td1}\square C^{Td3}$ (config. II) has a value that is larger by 50 % than B^{Td1}–C^{Td3} (config. I), which amounts to 6.05 eV/defect (table C.4, line 11). This is in wide contrast to the $(B_{12})C^iC^j$ model where the two configurations have quasi-identical formation enthalpy values (Section 3.1).

The formation enthalpy values of the two other in-plane configurations of the $(B_{12})C^iC^j$ model - configs. VII and VIII - are more than 1 eV/defect

greater than that of config. I (table C.4, lines 8–9). One can make the hypothesis that for config. I there is an interaction between C^{Td5} and C^{Td6} that is mediated by the icosahedron and lowers the formation enthalpy w.r.t. the two other in-plane configurations.

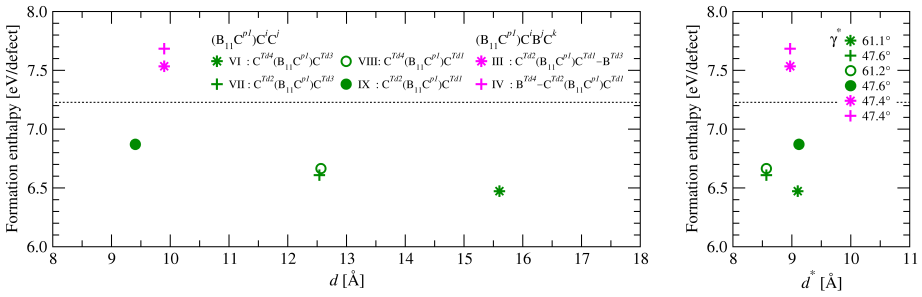

(a) (b)

Figure 7: Formation enthalpy of the $(B_{11}C^{p1})C^iC^j$ (dark green symbols) and $(B_{11}C^{p1})C^iB^jC^k$ (magenta symbols) models as a function of (a) d and ~~the distance between C^{Td} and $C^{Td'}$ atoms that are along the [111] direction;~~ (b) d^* defined in figure 6. ~~the distance between C^{Td} and C^{Td^*} atoms, where C^{Td^*} is defined as a $C^{Td'}$ atom in the neighboring supercell that makes the smallest C–C distance and that does not align with the C^{Td} atom along the [111] direction. The characterized angle $\angle C^{Td}OC^{Td^*}$ in each defect is shown in the legend.~~ γ^* is shown in the legend. Dotted line: the sum of formation enthalpy values, $H_f[(B_{11}C^p)] + 2H_f[(B_{12})C^{Td}]$, comparable to one ($B_{11}C^p$) and two ($B_{12}$)$C^{Td}$ defects that are totally isolated from each other.

Appendix D.2. Changing the (B_{12}) icosahedron to ($B_{11}C^p$)

Configurations of the $(B_{11}C^p)C^iC^j$ kind are characterized by the C^p–C^{Td} and the C^{Td}–$C^{Td'}$ distances. Unlike the C^p–C^{Td} distance (see Appendix E below), the C^{Td}–$C^{Td'}$ distance has a large effect on the formation enthalpy. For instance, the change amounts to 0.64 eV/defect between configs. I and IV, where the C^{Td2}–C^{Td4} distance varies from 1.64 Å to 2.80 Å (figure 3(b) of the main text, dark green point and square symbol). In figure 7(a), we observe dark green symbols that are distinct in formation enthalpy values w.r.t. the C^{Td}–$C^{Td'}$ distance along the [111] direction (configs. VI–IX). All of the dark green symbols lie below the dotted line, which indicates that we benefit in thermodynamical stability by a minimum of 0.36 eV/defect (config. IX) by aligning the interstitial carbon atoms along the [111] direction when we have ($B_{11}C^p$) instead of (B_{12}), w.r.t. the case where three carbon atoms are perfectly isolated.

The distance between two interstitial atoms has an even bigger effect in the $(B_{11}C^p)B^iC^j$ model (configs. V–VII), as a vacancy between interstitial boron and carbon atoms turns out to be highly unfavorable. Indeed, $B^{Td}\square C^{Td'}$ *Oh* vacancy case has its formation enthalpy value in the range

of 7.19±0.02 eV/defect (configs. V–VII). In particular, the formation enthalpy increases by 2.33 eV/defect while the B^{Td}–$C^{Td'}$ distance varies from 1.58 Å (config. I) to 3.00 Å (config. V).

Turning to the $(B_{11}C^{p1})C^iB^jC^k$ model, configs. I and II are quasi-equivalent in the formation enthalpy within 72 meV/defect, implying that the formation of a C^{Td}–B^{Oh}–$C^{Td'}$ bond is decisive in the relative stability of this defect, while the location of the C^p atom is negligible.

Finally, a boron atom at the *Td* position is forbidden with very high defect formation enthalpy (figure 7, magenta star and plus symbols & table C.4, lines 35–36).

Appendix E. Effect of the $\angle C^pOC^{Td}$ angle and the C^p–C^{Td} distance

Appendix E.1. Atomic models with one substitutional and one interstitial carbon atoms

In figure 8, we report the value of the formation enthalpy of neutral defects with one substitutional C^p and one interstitial C^{Td} atoms. The formation enthalpy is found to depend very weakly on the angle $\angle C^pOC^{Td}$ when the interstitial C^{Td} atom sits in the basal plane perpendicular to the [111] direction (figure 8(a)), and on the distance between C^p and C^{Td} when the C^{Td} atom sits along [111] (figure 8(b), see also table C.4).

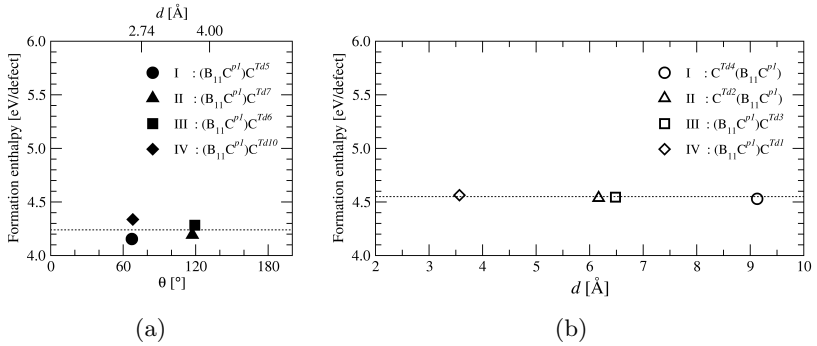

Figure 8: Formation enthalpy of the $(B_{11}C^p)C^i$ model as a function of (a) the angle defined by the C^{Td} atom, the icosahedron center, and the C^{Td} atom that is positioned in-plane, θ; (b) the distance between the C^p and C^{Td} atoms, *d*. The formation enthalpy values in panel (a) are within 4.24±0.09 eV/defect and the averge value is shown by the dotted line. The dotted line in panel (b) is the average value, 4.55 eV/defect.

Appendix E.2. Atomic models with one substitutional and two interstitial carbon atoms

Since the $(B_{11}C^p)C^iC^j$ model contains two interstitial carbon atoms, the C^p–C^{Td} distance can be characterized either as the C^p–C^{Td} or C^p–$C^{Td'}$

distance. Unlike the C^{Td}–$C^{Td'}$ distance, both the C^{p}–C^{Td} and the C^{p}–$C^{Td'}$ distances have a negligible effect (8 meV/defect) on the formation enthalpy of configs. I and II (figure 3(b) of the main text, dark green point and empty diamond symbol on the left), where the C^{p}–C^{Td} distance changes from 6.8 Å (C^{p}–C^{Td2}) to 4.2 Å (C^{p}–C^{Td1}) and the C^{p}–$C^{Td'}$ distance changes from 8.4 Å (C^{p}–C^{Td4}) to 5.8 Å (C^{p}–C^{Td3}). This is due to the formation of C^{Td}–$C^{Td'}$ bonds, namely C^{Td1}–C^{Td3} and C^{Td2}–C^{Td4} bonds, that make the atomic structure insensitive to the location of the substitutional atom in the icosahedron (see also table C.4, lines 24–25).
The same conclusion can be drawn by inspecting configs. IV and V that have a vacancy present between the C^{Td} and $C^{Td'}$ atoms: the magnitude of the change in the formation enthalpy is only 76 meV/defect as the C^{p}–C^{Td} and C^{p}–$C^{Td'}$ distances are either 6.24 Å and 9.01 Å, or 3.63 Å and 6.35 Å (table C.4, lines 27–28) (figure 3(b) of the main text, green square and cross symbols).
As the last example, the difference in formation enthalpy between configs. VII and VIII amounts to 55 meV/defect where the C^{p}–C^{Td} distance varies from 6.1 Å (C^{p}–C^{Td2}) to 3.5 Å (C^{p}–C^{Td1}) and the C^{p}–$C^{Td'}$ distance from 6.6 Å (C^{p}–C^{Td3}) to 9.2 Å (C^{p}–C^{Td4}) (figure 7, green plus and circle symbols & table C.4, lines 30–31).

Appendix E.3. Atomic models with one substitutional and three interstitial atoms

The configurations of the $(B_{11}C^{p})C^{i}B^{j}C^{k}$ kind are also characterized by the C^{p}–C^{Td} and C^{Td}–$C^{Td'}$ distances along the [111] direction, as in the previous section. Comparison between configs. I and II shows that C^{p}–C^{Td} and C^{p}–$C^{Td'}$ distances also have a small effect on formation enthalpy as in the previous section. For instance, in configs. I and II, the C^{p}–C^{Td} distance varies from 6.3 Å (C^{p}–C^{Td2}) to 3.7 Å (C^{p}–C^{Td1}) and the C^{p}–$C^{Td'}$ distance varies from 9.0 Å (C^{p}–C^{Td4}) to 6.4 Å (C^{p}–C^{Td3}), while the change in the formation enthalpy is only 72 meV/defect (figure 3(b), square and cross symbols in magenta).
In conclusion, the C^{p}–C^{Td} and C^{p}–$C^{Td'}$ distances have a minor effect on the formation enthalpy, in wide contrast with the C^{Td}–$C^{Td'}$ distance.

Appendix F. Formation enthalpy of charged defects

In figure 9, we report the formation enthalpy of charged defects as a function of the electronic chemical potential.

In the B-rich limit, the most stable defect atomic model turns out to be the positively charged $(B_{11}C^{p})$, then the neutral $(B_{12})C^{Td}$, and then the doubly-negatively charged $(B_{12})C^{Td1}$–C^{Td3}, with increasing electronic potential μ_e, from zero to E_g (Section 4). Turning to the C-rich limit, the most stable defect atomic model converts directly from the positively charged

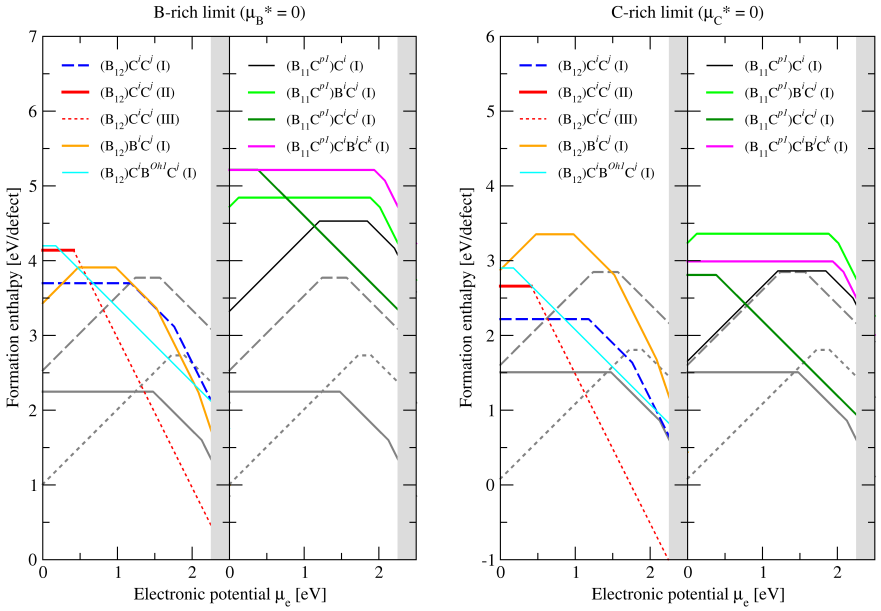

(a) (b)

Figure 9: Formation enthalpy of the charged defect as a function of the electronic potential within the band gap of pristine α boron. Excess chemical potential of B and C atoms fixed to that of the (a) B-rich and (b) C-rich limit obtained from the formation enthalpy of B_4C boron carbide. Dark grey curves for the simple defects (Appendix A): $(B_{11}C^p)$, dotted; $(B_{11}C^e)$, dashed; $(B_{12})C^{Td}$, solid. Colored curves: config. I of each defect atomic model, which has the lowest formation enthalpy when charge neutral. Exceptionally the $(B_{12})C^iC^j$ model is shown in three configurations (I–III). Left- and right-hand side of each panel: defect atomic models with unmodified (B_{12}) icosahedron and $(B_{11}C^p)$ icosahedron, respectively.

$(B_{11}C^p)$ to the doubly-negatively charged $(B_{12})C^{Td1}$–C^{Td3} at μ_e =1.1 eV (figure 9(b), left-hand side). The formation enthalpy of the doubly-negatively charged $(B_{12})C^{Td1}$–C^{Td3} in the C-rich limit is outstanding. Its value at the CBM (−1.02 eV) implies that a doubly-negatively charged C^{Td}–$C^{Td'}$ bond could be even more stable than the pristine α boron.

In table F.5, we report the formation enthalpy of charged defects in some of the configurations at the B-rich limit.

In table F.6, we report interatomic distances that are the main geometric parameters in this study, within the defect atomic models and configurations that are listed in table F.5, while the defects with one carbon atom are excluded since the geometric parameters become irrelevant. A large decrease in C^{Td}–$C^{Td'}$ distance is observed in config. II of the $(B_{12})C^{Td}C^{Td'}$ defect, as it is 3.13 Å in the charge-neutral state and 1.70 Å in the doubly-negatively charged ($q = -2$) state, which indicates the formation of a C^{Td}–$C^{Td'}$ bond.

Model	Config.	Charge state q (e)				
		-2	-1	0	$+1$	$+2$
α boron (Ref.)				0		
One substitutional C atom						
$(B_{11}C^{p})$		7.10	4.63	2.73	1.01	1.32
$(B_{11}C^{e})$		7.80	5.34	3.77	2.53	2.89
Single-atom interstitial						
$(B_{12})C^{Td}$		5.85	3.73	2.25	2.35	
Two-atom interstitial						
$(B_{12})C^{Td}C^{Td'}$	I	6.64	4.88	3.70	3.88	
	II	4.96	4.97	4.14	4.39	
	III	5.09	4.42	4.21	4.42	
	VI	7.73	5.90	4.58	4.78	
	VIII	7.72	6.01	4.90	5.10	
$(B_{12})B^{Td}C^{Td'}$	I	6.41	4.89	3.43	3.91	
Three-atom interstitial						
$(B_{12})C^{Td}B^{Oh1}C^{Td'}$	I	6.76	4.37	4.20	4.53	
One substitutional C atom & Single-atom interstitial						
$(B_{11}C^{p})C^{Td}$	I	8.58	6.38	4.53	3.32	
One substitutional C atom & Two-atom interstitial						
$(B_{11}C^{p})B^{Td}C^{Td'}$	I	8.74	6.73	4.84	4.72	
	II	8.68	6.78	4.96	4.88	
$(B_{11}C^{p})C^{Td}C^{Td'}$	I	7.89	5.60	5.22	5.27	
	II	7.87	5.59	5.22	5.29	
One substitutional C atom & Three-atom interstitial						
$(B_{11}C^{p})C^{Td}B^{j}C^{Td'}$	I	9.23	7.15	5.21	5.37	
	II	9.14	7.19	5.28	5.44	

Table F.5: Defect formation enthalpy (eV) at the B-rich limit as a function of the charge state ranging from -2 to $+1$ (or $+2$). The electronic potential was fixed to $\mu_e = 0$. When possible, the names of the sites $p/Td/Oh$ have been directly inserted into the model name instead of using the i, j, and k indices of table 1.

Model	Config.		Charge state q (e)			
			-2	-1	0	$+1$
Two-atom interstitial						
$(B_{12})C^{Td}C^{Td'}$	I	Td–Td'	3.05	3.02	3.00	3.00
	II	Td–Td'	1.70	2.80	3.13	3.13
	III	Td–Td'	1.69	1.65	1.60	1.57
	VI	Td–Td'	9.54	9.42	9.31	9.31
	VIII	Td–Td'	5.92	5.91	5.90	5.90
$(B_{12})B^{Td}C^{Td'}$	I	Td–Td'	1.62	1.57	1.52	1.48
Three-atom interstitial						
$(B_{12})C^{Td}B^{Oh1}C^{Td'}$	I	Td–Td'	2.80	2.79	2.79	2.80
One substitutional C atom & Single-atom interstitial						
$(B_{11}C^{p})C^{Td}$	I	p–Td	9.14	9.04	9.13	9.23
One substitutional C atom & Two-atom interstitial						
$(B_{11}C^{p})B^{Td}C^{Td'}$	I	p–Td	5.69	5.62	5.56	5.52
		p–Td'	4.06	4.03	4.01	4.00
		Td–Td'	1.67	1.61	1.58	1.54
	II	p–Td	4.27	4.33	4.39	4.44
		p–Td'	5.90	5.92	5.95	5.97
		Td–Td'	1.67	1.61	1.57	1.54
$(B_{11}C^{p})C^{Td}C^{Td'}$	I	p–Td	6.77	6.78	6.80	6.83
		p–Td'	8.45	8.45	8.42	8.39
		Td–Td'	1.69	1.69	1.64	1.57
	II	p–Td	4.15	4.14	4.16	4.19
		p–Td'	5.80	5.79	5.77	5.73
		Td–Td'	1.69	1.69	1.64	1.57
One substitutional C atom & Three-atom interstitial						
$(B_{11}C^{p})C^{Td}B^{j}C^{Td'}$	I	p–Td	6.28	6.26	6.26	6.26
		p–Td'	9.05	9.03	9.03	9.03
		Td–Td'	2.79	2.79	2.80	2.80
	II	p–Td	3.65	3.66	3.65	3.65
		p–Td'	6.38	6.39	6.39	6.38
		Td–Td'	2.79	2.79	2.79	2.80

Table F.6: Distance between two carbon atoms (Å) in selected configurations from table F.5. When possible, the names of the sites $p/Td/Oh$ have been directly inserted into the model name instead of using the i, j, and k indices of table 1.

References

[1] T. Ogitsu, F. Gygi, J. Reed, Y. Motome, E. Schwegler, and G. Galli, "Imperfect crystal and unusual semiconductor: Boron, a frustated element," J. Amer. Chem. Soc., vol. 131, p. 1903, 2009.

[2] G. Roma, K. Gillet, A. Jay, N. Vast, and G. Gutierrez, "Understanding first order Raman spectra of boron carbides across the homogeneity range," Phys. Rev. Mat., vol. 5, p. 4063601, 2021. [Online]. Available: https://doi.org/10.1103/PhysRevMaterials.5.063601

[3] G. Roma, A. Jay, N. Vast, O. H. Duparc, and G. Gutierrez, "Reply to "comment on 'understanding first order raman spectra of boron carbides across the homogeneity range," Phys. Rev. Mat., vol. 6, p. 016602, 2022. [Online]. Available: https://doi.org/10.1103/PhysRevMaterials.6.01660

[4] A. Jay, O. H. Duparc, J. Sjakste, and N. Vast, "Theoretical raman spectrum of boron carbide $B_{4.3}C$ under pressure," Acta Materialia, vol. 255, p. 119085, 2023.

[5] A. Chakraborti, Y. Cho, J. Sjakste, B. Baptiste, L. Henry, N. Guignot, Y. Le Godec, and N. Vast, "When carbon impurities trigger the synthesis of alpha boron at high pressure and high temperature," Acta Materialia, vol. 249, p. 118820, 2023.

[6] F. Horn, "Some electrical and optical properties of simple rhombohedral boron," Journal of Applied Physics, vol. 30, p. 1611, 1959.

[7] B. F. Decker and J. S. Kasper, "The crystal structure of a simple rhombohedral form of boron," Acta Crystallographica, vol. 12, pp. 503 – 506, 1959.

[8] B. Albert and H. Hillebrecht, "Boron: Elementary challenge for experimenters and theoreticians," Angew. Chem., vol. 48, p. 8640, 2009.

[9] G. Parakhonskiy, N. Dubrovinskaia, L. Dubrovinsky, S. Mondal, and S. van Smaalen, "High pressure synthesis of single crystals of alpha-boron," Journal of Crystal Growth, vol. 321, pp. 162–166, 2011.

[10] E. Amberger, W. Stumpf, and K. Buschbeck, "Boron compounds, elemental boron and boron carbides," in Gmelin Handbook of Inorganic Chemistry. Berlin: Springer-Verlag, 1981, vol. 13 Suppl. 2.

[11] G. Parakhonskiy, N. Dubrovinskaia, E. Bykova, R. Wirth, and L. Dubrovinsky, "Experimental pressure-temperature phase diagram of boron: resolving the long-standing enigma," Scientic Reports, vol. 96, p. 1, 2011.

[12] S. Gunji, H. Kamimura, and T. Nakayama, "Electronic structures of newly predicted intercalation compounds "lithium intercalated α-boron"," Journal of the Physical Society of Japan, vol. 62, no. 7, pp. 2408 – 2418, 1993.

[13] S. Gunji and H. Kamimura, "*First-principles* study on metal-doped icosahedral B_{12} solids," Phys. Rev. B, vol. 54, p. 13665, 1996.

[14] K. Soga, A. Oguri, S. Araake, M. Terauchi, A. Fujiwara, and K. Kimura, "Li- and Mg-doping into icosahedral boron crystals, α- and β-rhombohedral boron, targeting high-temperature superconductivity: structure and electronic states," Journal of Solid State Chemistry, vol. 177, p. 498, 2004.

[15] W. Hayami, T. Tanaka, and S. Otami, "Theoretical study of the stability of lithium atoms in α-rhombohedral boron," The Journal of Physical Chemistry A, vol. 109, pp. 11 975 – 11 979, 2005.

[16] H. Dekura, K. Shirai, and H. Katayama-Yoshidai, "Valence control of α-rhombohedral boron by electronic doping," J. Phys.: Cond. Matter, vol. 19, p. 365241, 2007.

[17] H. Dekura, K. Shirai, and A. Yanase, "Efficient method for Li doping of α-rhombohedral boron," Phys. Rev. B, vol. 84, p. 094117, 2011.

[18] ——, "Metallization of α-boron by hydrogen doping," Journal of Physics: Conference Series, vol. 176, p. 012005, 2009. [Online]. Available: https://doi.org/10.1088/1742-6596/176/1/012005

[19] G. A. Slack, "Thermal conductivity of elements with complex lattices: B, p, s," Phys. Rev., vol. 139, p. A507, 1965.

[20] M. Widom and M. Mihalkovič, "Symmetry-broken crystal structure of elemental boron at low temperature," Phys. Rev. B, vol. 77, p. 064113, 2008.

[21] D. Bylander, L. Kleinman, and S. Lee, "Self-consistent calculation of the energy bands and bonding properties of $B_{12}C_3$," Phys. Rev. B, vol. 42, p. 1394, 1990.

[22] O. Chauvet, D. Emin, L. Forro, T. Aselage, and L. Zuppiroli, "Spin susceptibility of boron carbides: Dissociation of singlet small bipolarons," Phys. Rev. B, vol. 53, p. 14450, 1996.

[23] M. Widom and W. Huhn, "Prediction of orientational phase transition in boron carbide." Sol. St. Sc., vol. 14, p. 1648, 2012.

[24] K. Gillet, G. Roma, J.-P. Crocombette, and D. Gosset, "The influence of irradiation induced vacancies on the mobility of helium in boron carbide," Journal of Nuclear Materials, vol. 512, pp. 288–296, 2018. [Online]. Available: https://www.sciencedirect.com/science/article/pii/S0022311518310286

[25] A. Chakraborti, N. Guignoy, N. Vast, and Y. Le Godec, "Synthesis of boron carbide from its elements up to 13 GPa," Journal of Physics and Chemistry of Solids, vol. 159, p. 110253, 2021.

[26] The formation enthalpy value of a ($B_{10}C_2$) icosahedron in the 3×3×3 supercell ranges from 4.78 to 6.44 eV/defect. The difference between the smallest formation enthalpy value of two-carbon-atom interstitial defect and the smallest formation enthalpy value of two-carbon-atom substitutional defect equals to 1.1 eV/defect.

[27] J. Perdew and Y. Wang, "Accurate and simple analytic representation of the electron-gas correlation energy," Phys. Rev. B, vol. 45, p. 13244, 1992.

[28] A. Jay, O. H. Duparc, J. Sjakste, and N. Vast, "Theoretical phase diagram of boron carbide from ambient to high pressure and temperature," J. Appl. Phys., vol. 125, p. 01, 2019, special edition on Ultra-Hard Materials.

[29] M. Methfessel and A. Paxton, "High-precision sampling for Brillouin-zone integration in metals," Phys. Rev. B, vol. 40, p. 3616, 1989.

[30] H. Monkhorst and J. Pack, "Special points for Brillouin-zone integrations," Phys. Rev. B, vol. 13, p. 5188, 1976.

[31] G. A. Baraff and M. Schlüter, "Electronic structure, total energies, and abundances of the elementary point defects in gaas," Phys. Rev. Lett., vol. 55, p. 1327, 1985.

[32] S. B. Zhang and J. E. Northrup, "Chemical potential dependence of defect formation energies in gaas: Application to ga self-diffusion," Phys. Rev. Lett., vol. 67, p. 2339, 1991.

[33] J. Pruneda and E. Artacho, "Energetics of intrinsic point defects in $ZrSiO_4$," Phys. Rev. B, vol. 71, p. 094113, 2005.

[34] J. T. Schick and C. G. Morgan, "Gallium interstitial contributions to diffusion in gallium arsenide," AIP Adv., vol. 1, p. 032161, 2011.

[35] R. Ramprasad, H. Zhu, P. Rinke, and M. Scheffler, "New perspective on formation energies and energy levels of point defects in nonmetals," Phys. Rev. Lett., vol. 108, p. 066404, 2012.

[36] R. Raucoules, N. Vast, E. Betranhandy, and J. Sjakste, "Mechanical properties of icosahedral boron carbide explained from *first principles*," Phys. Rev. B, vol. 84, p. 014112, 2011.

[37] The second order polynomial fit has been obtained as: $y = -9.16 \times 10^{-5}(x - 180)^2 + 5.00$, where the variables x and y stand for the angle $\angle \mathrm{C}^{Td}\mathrm{OC}^{Td'}$ [°] and the formation enthalpy [eV/defect], respectively. The maximum point has been set to be at $x = 180(^\circ)$.

[38] F. Bruneval, C. Varvenne, J.-P. Crocombette, and E. Clouet, "Pressure, relaxation volume, and elastic interactions in charged simulation cells," Physical Review B, vol. 91, p. 024107, 2015.

[39] The atomic volume has been defined as the supercell volume divided by the total number of atoms, which includes the inserted carbon and boron atoms.

[40] R. Lazzari, N. Vast, J. Besson, S. Baroni, and A. D. Corso, "Structural and vibrational properties of icosahedral B_4C boron carbide," Phys. Rev. Lett., vol. 83, no. 16, p. 3230, 1999.

[41] V. Domnich, S. Reynaud, R. Haber, and M. Chhowalla, "Boron carbide: Structure, properties, and stability under stress," J. Am. Ceram. Soc., vol. 94, p. 3605, 2011.

[42] E. Betranhandy, N. Vast, and J. Sjakste, "*Ab initio* study of defective chains in icosahedral boron carbide B_4C," Solid State Sciences, vol. 14, p. 1683, 2012.

[43] A. Jay, "*In silico* design of a new phase of boron carbide (in french)," Ph.D. dissertation, École Polytechnique, Palaiseau, France, 2015. [Online]. Available: https://pastel.archives-ouvertes.fr/tel−01199235/file/These_Jay.pdf

[44] C. E. Dreyer, A. Alkauskas, J. L. Lyons, A. Janotti, and C. G. V. D. Walle, "First-Principles Calculations of Point Defects for Quantum Technologies," Annu. Rev. ofMaterials Res., vol. 48, pp. 1–26, 2018.

[45] The band gap of pristine α boron has been calculated using the HSE06 hybrid exchange–correlation functional, between the CBM at F and VBM at Z [5].

[46] P. Giannozzi, O. Andreussi, T. Brumme, O. Bunau, M. B. Nardelli, M. Calandra, R. Car, C. Cavazzoni, D. Ceresoli, M. Cococcioni, N. Colonna, I. Carnimeo, A. D. Corso, S. de Gironcoli, P. Delugas, R. A. D. J. A. Ferretti, A. Floris, G. Fratesi, G. Fugallo, R. Gebauer, U. Gerstmann, F. Giustino, T. Gorni, J. Jia, M. Kawamura, H.-Y.

Ko, A. Kokalj, E. Küçükbenli, M. Lazzeri, M. Marsili, N. Marzari, F. Mauri, N. L. Nguyen, H.-V. Nguyen, A. O. de-la Roza, L. Paulatto, S. Poncé, D. Rocca, R. Sabatini, B. Santra, M. Schlipf, A. P. Seitsonen, A. Smogunov, I. Timrov, T. Thonhauser, P. Umari, N. Vast, X. Wu, and S. Baroni, "Advanced capabilities for materials modelling with QUANTUM ESPRESSO," J. Phys.: Condens. Matter, vol. 29, p. 465901, 2017. [Online]. Available: http://www.quantum-espresso.org

[47] K. Rasim, R. Ramlau, A. Leithe-Jasper, T. Mori, U. Burkhard, H. Borrmann, W. Schnelle, C. Carbogno, M. Scheffler, and Y. Grin, "Local atomic arrangements and band structure of boron carbide," Angew. Chem., vol. 130, p. 1, 2018.